# Cavity Ring-Down Spectroscopy (CRDS) Measurements of Barium Emitted from a Hollow Cathode

Seth Antozzi[1], Jacob Gottfried[1], John Williams[2], Azer P. Yalin[3]

*Colorado State University, Fort Collins, CO, 80523, USA*

**Hollow cathodes (HC) are important components of several electric propulsion devices acting as electron sources and neutralizers. Widely used barium oxide (BaO) HCs are prone to evaporation and sputtering due to plasma-heating and collisions of ions within the channel of the HC. Measuring the number density of the barium atoms that are emitted in the plasma plume of the HC will help inform models of HC physics and lifetime. In this work, cavity ring-down spectroscopy (CRDS) measurements of barium from the thermionic emitter of a heaterless BaO HC are presented. The CRDS scheme employs a pulsed laser at ~553.7 nm (vacuum wavelength) to access a ground state transition of barium and allows a Ba density detection limit of ~4x10^5 cm^-3. We have performed spatial scans of barium density within the plasma plume at a position 0.5 cm downstream from the orifice of the cathode at a current of 5 A and flow-rate of 10 sccm. An Abel inversion was used to find radial Ba density yielding a peak value of ~1.8x10^6 cm^-3. We have also performed initial measurements of barium density versus axial distance, anode current, and krypton flow.**

## I. Introduction

For outer space missions such as NASA's Artemis, electric propulsion (EP) systems are becoming more popular due to their high specific impulse (ISP) and overall excellent thrust-to-weight ratios. An important component of these propulsion systems is the hollow cathode (HC) which serves as an electron source for the thruster and/or to neutralize the emitted beam. Popular emitter materials for these HCs are barium oxide (BaO) and lanthanum hexaboride (LaB$_6$) due, in part, to their resilience against erosion and contamination. However, the chemical processes that govern the electron emitter surface chemistry evolution and operating temperature are still largely unknown [1,2]. A key measurement necessary to understand these processes is the quantification of the neutral and ion erosion products in the plasma, both internal to the HC and in its emitted plume downstream of the orifice. This knowledge, combined with results from simulation codes, will enable prediction of emitter erosion and cathode lifetime.

Our focus is on advancing methods to quantify barium neutrals evolved from BaO cathodes. Quantitative diagnostics of barium in the plasma presents two major challenges: the extreme dilution of barium (neutrals and ions) in the plasma which requires extreme measurement sensitivity, and the lack of access to the interior plasma region given the compact geometry of the cathode assembly. Cavity Ring-Down Spectroscopy (CRDS) is a promising technique to address these two constraints and enable the critical measurements of Ba species in the cathode inner region and plume. The present submission builds upon our work applying CRDS to fundamental studies of sputtered metals as well as (near) real-time measurements of sputtered boron densities from the channel of an operating Hall thruster [3-11].

In this study we use CRDS as a detection technique for barium evolved from the thermionic emitter of a heaterless, custom-built BaO HC. The layout of the remainder this paper is as follows: the optical layout and cathode setup are

---

1. Grad. Student, Dept. of Mech. Engineering, Colorado State University, Fort Collins, CO, Member AIAA
2. Professor, Dept. of Mech. Engineering, Colorado State Univ., Fort Collins, CO, Member AIAA
3. Professor, Dept. of Mech. Engineering, Colorado State Univ., Fort Collins, CO, Associate Fellow AIAA

presented in section II. The CRDS technique and analysis methods are explained in section III, while section IV contains experimental results, and section V gives conclusions and future work.

## II.  Experimental Setup

Our CRDS scheme for Ba detection is based on probing a strong absorption line at ~553.7 nm (vacuum) originating from the ground-state.  Using a line that originates from the ground state is important for a robust population estimate since such transitions describe a very large (and temperature insensitive) fraction of the overall population. The optical setup used for our HC CRDS is shown in Figure 1. On the air side, the laser beam is produced by an ND:YAG laser (Continuum Powerlite 8010) pumping a dye laser (Sirah CobraStretch) using pyrromethene 580 dye (ethanol solvent) that is tuned to ~553.7 nm. Although CRDS can use a continuous-wave (c-w) laser, this study uses a pulsed laser in order to avoid the complexities of mode-matching, and the need to extinguish the beam with a fast-modulator and trigger, as are needed in cw-CRDS. The laser energy intensity is controlled by the variable attenuator, which includes a half-wave plate, iris, and polarization cube. The iris acts as a spatial filter to clean up the spatial mode of the beam. Additional spatial filtering is provided by a spatial filter that uses a 1:4 de-magnifying telescope and a pinhole filter [12]. Using the spatial filter and iris allow us to reduce noise (shot-to-shot variations) in the ring-down signals. The resulting beam is focused to a waist, roughly coinciding with the center of the cavity (in the ~60 cm$^3$ spherical vacuum chamber), using a 500 mm plano-convex lens. The optical cavity is formed from two high-reflectivity (HR) mirrors and is 99.7 cm long including extender arms on either side (length 16.5 cm).  The arms serve to protect the HR mirrors by increasing their distance to the cathode and its plasma.  They also include ~6 and 10 mm diameter hole baffles (2 baffles in each arm) that reduce the opportunity for sputtered particles (and other possible contaminants) to reach the HR mirror surfaces. The beam exiting the optical cavity is measured with a photomultiplier tube (PMT, Hamamatsu R9110) that includes a fast transimpedance amplifier.  A bandpass filter (Edmunds 550-10) is placed in front of the PMT to minimize detection of plasma luminosity and other light that may interfere with the ring-down signals or saturate the PMT. The PMT is generally operated at 450 volts for this study, with a gain of ~7x10$^4$. This voltage and gain-level may be outside the linear regime of the PMT, which we will check more in the future; however, the exponential nature of the ring-downs suggests this was not a significant problem. The resulting ring-down decay signal is analyzed using a custom Labview program that fits a ring-down time, $\tau$, to each (single-shot) decay.  For wavelength scans, the laser is scanned continuously from 553.694 nm to 553.710 nm with scan speed of 0.005 nm/minute. The ring-down signals are collected and fitted individually to the exponential decay curve with a custom Labview code and then are grouped into 50 point averages (50 laser shots) to improve signal-to-noise. At each wavelength position, the resulting 50 $\tau$ values are averaged to give a final $\tau$ value.



1: Nd:YAG pump beam
2: Dye Laser
3: Focusing Lens
4: Steering Mirror
5: Photodiode Trigger
6: Spatial Filter
7: Variable Attenuator
8: HR Mirror
9: Baffles
10: BaO Hollow Cathode
11: Anode
12: PMT
13: Oscilloscope
14: Computer
15: Vacuum Chamber
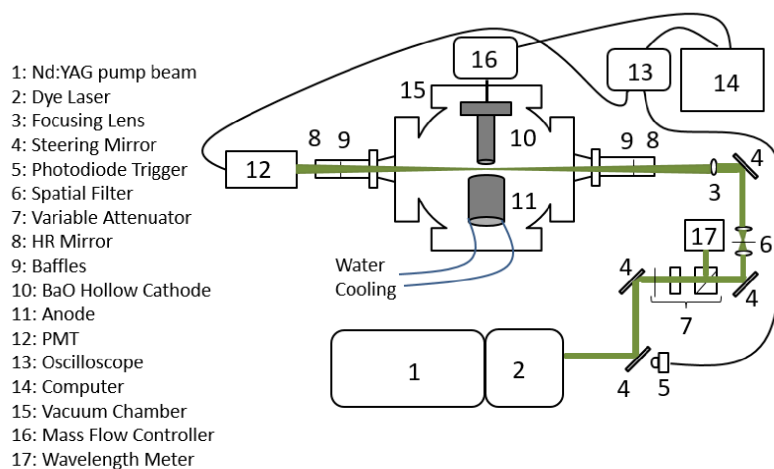16: Mass Flow Controller
17: Wavelength Meter

**Fig. 1** Optical layout of CRDS experiment.

The CRDS laser beam probes the HC plasma plume shown in Figure 2. The HC is a heaterless, BaO cathode custom-built by the CSU Electric Propulsion and Plasma Engineering (CEPPE) laboratory, using a hollow, circular anode. The HC runs on krypton, using a mass flow controller (Brooks GF120 Mass Flow Controller), which gives a range of ~3-40 SCCM gas flow rates. The HC keeper power supply is set at a constant 1 A for the keeper, and a range of currents of ~5-12.5 A for the anode, with variable voltages, generally around 10.8 V for the keeper, and 38 V for the anode. The vacuum chamber uses a roughing pump and an Agilent TV 1001 turbomolecular pump, with a base pressure of $\sim10^6$ torr. When the flow rate of 5.0 SCCM is used, the chamber pressure is about 0.3 mTorr. The HC is oriented in the chamber as shown in figure 2, on a translation stage with two degrees of freedom to enable fine position adjustments without breaking vacuum. We define a cylindrical $(r,z)$ coordinate scheme based on the axisymmetric cathode with $r=0$ on the centerline, and $z=0$ at the HC orifice plate (and larger values of $z$ extending axially into the plume). In our study, the motion stage is used for radial scans from $r \sim$0-1 cm (in both radial directions), with the other stage allowing axial movement from $z$ of ~0.25-3 cm.
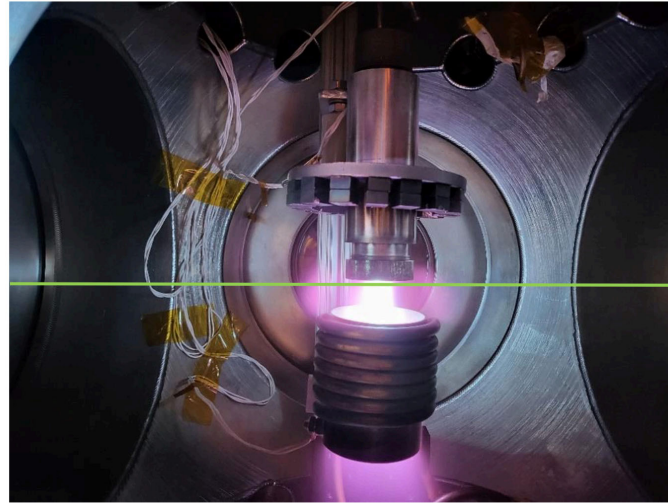


**Fig. 2** Hollow cathode with running plasma, with green line representing the position of the probing laser beam.

## III.   CRDS Data Analysis

CRDS is a laser absorption technique based upon the Beer Lambert Law relating light transmission to the absorbing properties of a sample (Ba atoms in our case). A key feature of CRDS is that it achieves very high sensitivity (i.e., ability to measure low densities) by exploiting the very long effective path length provided by housing the absorption sample within a high-reflectivity optical cavity. The CRDS method works by measuring the optical decay (ring-down) time of light in the cavity, from which the sample absorption can be found. Because a temporal decay rate is measured, the technique is also relatively insensitive to laser power fluctuations which can limit other absorption approaches. In a typical CRDS experiment, as seen in figure 3, the incident laser beam enters the optical cavity, then bounces back and forth many times, yielding the decay in output light intensity:

$$I_{out} = I_0 \exp\left[-\frac{t}{\tau_0}\right], \text{ where } \tau_0 = \frac{L}{(1-R)c} \tag{1}$$

where $I_{out}$ is the decaying beam intensity exiting the cavity, $L$ is the cavity length,, $I_0$ is the initial beam intensity, $t$ is time, $R$ is reflectivity, $c$ is speed of light, and $\tau_0$ is the "empty-cavity ring-down time" (i.e., the ring-down time with no absorbing sample present, or with the laser detuned from the absorption line) [13].

When an absorber is present, the ring-down time, $\tau$, can be related to the cavity loss as:

$$\frac{1}{\tau(v)} = \frac{c}{L}\left[\int k(c,v)dx + (1-R)\right] \tag{2}$$

where $k$ is the absorption coefficient and $v$ is the laser frequency [10]. Equation (2) allows for a varying concentration of the absorbing sample over the length of the sample volume. The expression 1-$R$ represents the loss from the mirrors, including scattering [10]. If the laser lineshape is given as $L(v)$, then the effective absorption coefficient that includes line broadening can be given as a convolution of the lineshape with the absorption profile:

$$k_{eff}(v) = \int_{-\infty}^{\infty} dv' L(v'-v)k(v'). \tag{3}$$

Considering both $\tau_0$ and $\tau$, the effective (dimensionless) sample absorbance $abs_{eff}$ and effective absorption coefficient $k_{eff}$ can be found (generally by detuning the laser), as:

$$abs_{eff}(v) = l_{abs}k_{eff}(v) = \frac{l}{c}\left[\frac{1}{\tau(v)} - \frac{1}{\tau_0}\right] \tag{4}$$

where $l_{abs}$ is the length of the absorption volume.

Based on equation (1), the ring-down time with an absorbing sample decreases relative to the empty-cavity ring-down time, giving a signal representing the number density of the sample present. A common method to measure sample number density (actually path-integrated density) is to the scan the laser across the absorbing feature, measuring $\tau(v)$, and then to (frequency-) integrate the area of the absorbance spectrum. Using the spectroscopic constants (for a transition from lower-state $i$ to upper-state $k$,) then allows determination of the path-integrated number density:

$$\int N_i dx = 8\pi \frac{g_i}{g_k} \frac{v_{ki}^2}{A_{ki}c^2}\left[\int abs_{eff}(v)dv\right] \tag{5}$$

where $\int N_i dx$ is the number density integrated along the beam, $g_i$ and $g_k$ are degeneracies, $v_{ki}$ is the transition frequency, and $A_{ki}$ is the Einstein coefficient of the transition [10]. For our specific transition, the values of the spectroscopic parameters are as follows: $g_i = 1$, $g_k = 3$, $A_{ki} = 1.19 \times 10^8\ s^{-1}$, $v_{ki} = 5.41 \times 10^{14}$ Hz [14].

The experiments presented herein determine path-integrated Ba densities following the above method with eqn. (5). In some cases we also determine local spatially-resolved (radially dependent) number densities, i.e. in units of cm$^{-3}$ versus cm$^{-2}$, assuming that the plasma is axisymmetric about the cathode axis. For this purpose, we perform spatial CRDS scans in the transverse direction, by using the translation stage to offset the laser axis to different radial positions (relative to the cathode center-line), and then use a Fourier-based Abel inversion code to infer the radially dependent densities from the path-integrated measurement [15].
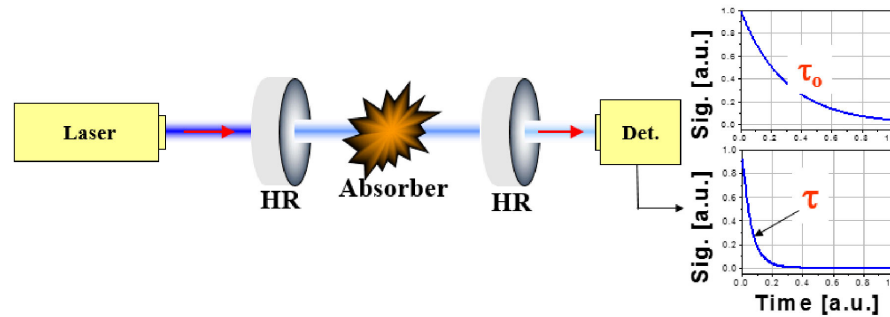


**Fig. 3** Illustration of a CRDS 2-mirror optical cavity with resulting ring-down decay profiles on right.

## IV.  Results and Discussion

### A. Acquisition of Ring-Down Signals and Analysis of Wavelength Scans

For CRDS ring-down signal acquisition, we first examine signals arising from the "empty-cavity" without the cathode operating.  Ring-down decays are measured using the methodology explained in the last section. We observe typical values of empty-cavity ring-down time of ~20 μs corresponding to mirror reflectivity of 0.99983 using equation (1) which is roughly consistent with manufacturer specifications and past experiments with the same mirrors.

Figure 4 shows an example CRDS absorbance spectrum, in units of parts-per-million (ppm), with the cathode operating. Unless otherwise indicated, the experiments were done with HC anode current of 5 A and krypton flow rate of 10 sccm. Part of the motivation for this choice of operating conditions was managing plasma degradation of ring-down signals to facilitate more consistent experimental results. The plotted (effective) absorbance is calculated with eqn. (4) and is after baseline ($\tau_0$) subtraction. The spectrum was recorded at axial position of $z$=5 mm and radial position of $r$ = -1 mm. The laser scan is over ~16 GHz extent and the  spectral absorption peak has a full-width-half-maximum (FWHM) of ~2.2 GHz based on a Voigt fit to the spectrum ($R^2$=0.98). Each data-point is assigned an uncertainty of ±10% based on a conservative estimation of experimental reproducibility of ring-down times.
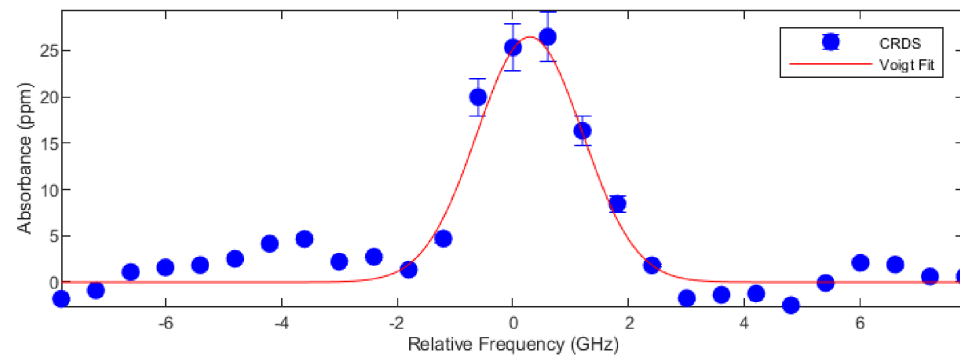


**Fig. 4** Example CRDS wavelength scan recorded at axial position of $z$=5 mm and radial position of $r$=-1 mm. HC conditions are 5 A, 10 sccm.

### B. Spatial Scans and Radial Density Profiles

In accordance with equation (5), we have performed (line-integrated) CRDS measurements across a series of chords, by displacing the translation-stage in the $r$-direction, at $z$ = 5 mm below the orifice plate. The displacements spanned approximately 1 cm to either side (with step-size of 1 mm).  The HC was again operated with krypton flow of 10 sccm and anode current of 5 A. The path-integrated number density of barium as function of the radial position is shown in Figure 5. We report an uncertainty of ±20% on the measured densities based on experimental reproducibility (of path-integrated results). As expected, the data peak close to the radial center line and are relatively symmetric about $r$=0.  We use a Gaussian fit as a convenient means to approximate the spatial shape though there is no theoretical underpinning for this choice. The error in the radial direction is ±0.25 mm, based on the translation stage in use.
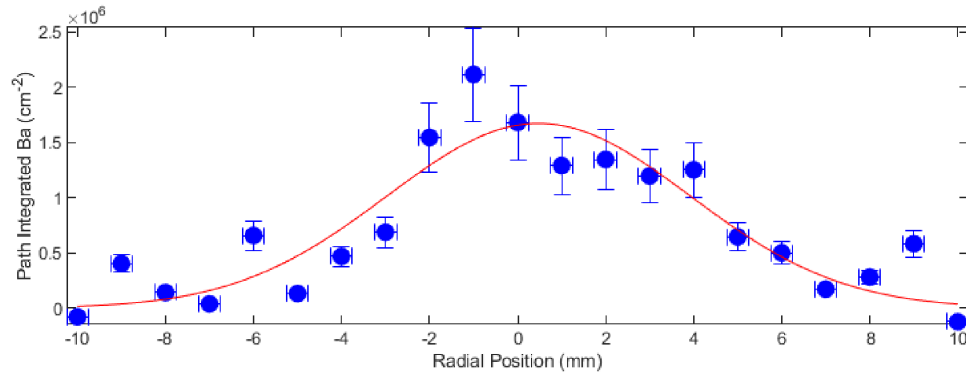
**Fig. 5** Path-integrated barium as function of transverse (radial) position for 5 A, 10 sccm.

The data from the Gaussian fit was used for an Abel inversion, in which the (fitted) path-integrated barium at each evenly-spaced 1 mm step radial location is fed into the Abel inversion function. We use the data from the Gaussian fit for the inversion, as opposed to the raw-data, to reduce measurement noise and enforce symmetry. Figure 6 shows the resulting Ba densities calculated at each radial location, in which symmetry in the (-) side is assumed.

The resulting full width, half max (FWHM) of the Abel-inverted radial density profile is 9.0 mm. This FWHM is used throughout the rest of the paper as a representative path-length for simple determination of (peak) Ba density from path-integrated Ba density (i.e., for cases when measurements are performed only at $r$=0 without full spatial scan). Based on these data, we estimate a detection limit for Ba density of ~4x10$^5$ cm$^{-3}$ based on the observed peak density and signal-to-noise ratio (SNR) of ~5.
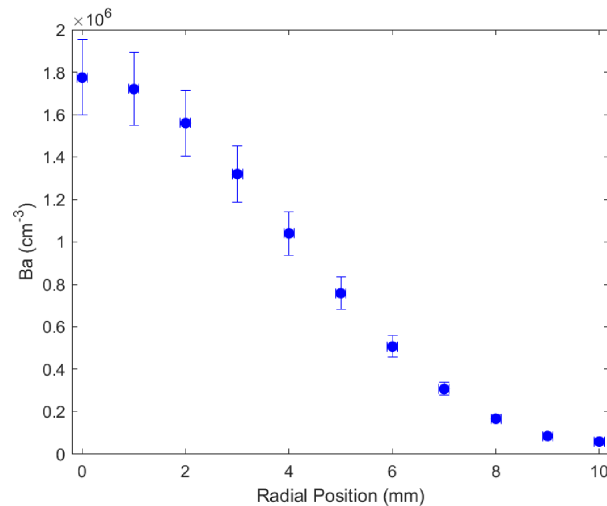
.



**Fig 6** Radial profile of barium density found with Abel inversion of spatially scanned data (Fig. 5).

A further study of barium density was done by varying the height of the HC in reference to the probe beam and using the wavelength scanning method to measure the Ba density as a function of axial position $z$ (with step-size 2.5

mm). Here, since no radial scans were done, the path-integrated method (at $r$=0) was paired with a path length of 9.0 mm for barium density calculations, as discussed above. The cathode was operated with krypton flow of 10 sccm and current of 5 A. The results are shown in Figure 7 with largest signals observed at the smallest $z$ values, i.e., closest to the cathode keeper orifice. This method of analysis does not account for possible changes in the shape of the radial profile (which may vary with different axial positions and HC conditions). Future work can further explore the HC barium radial profiles. Error here is again ±20% in the Ba density, based as before on experimental reproducibility. The assumed error of the positions is quite small, ±0.25 mm, again based on the accuracy of the translation stage system.
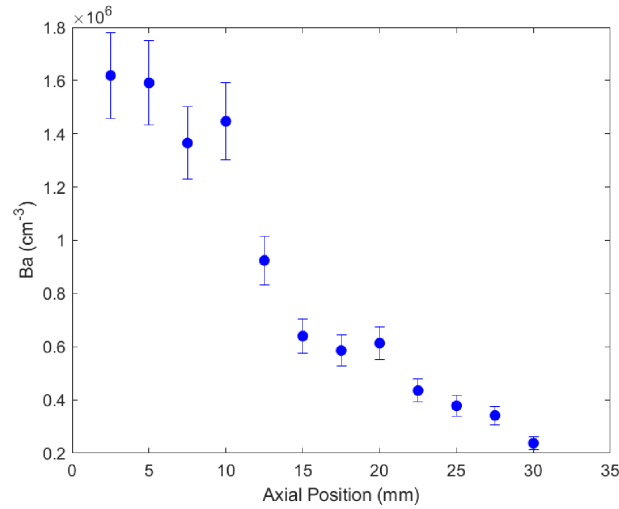


**Fig. 7** Axial profile of barium density at $r = 0$ and cathode operation at 10 sccm and 5 A.

## C. Dependence of Ba Density of Cathode Current and Flow rate

Barium density variation as a function of the anode current and flow rate were considered. In the left of figure 8, the variation in Ba density over a series of current (stepping at 2.5 A increments) is shown. The data shows a gradual increase likely due to greater barium emission, followed by a larger increase from 10 to 12.5 A. The flow and position were held constant at 10 sccm, and $r = 0$ mm, $z = 5$ mm, respectively. A similar radial distribution and FWHM (9.0 mm) are assumed for the path integration method, since no radial scans were done at these parameters. The right of Figure 8 shows the spectral scans (after baseline subtraction) for the current variation study. The FWHM of the spectra remain uniform within experimental error.
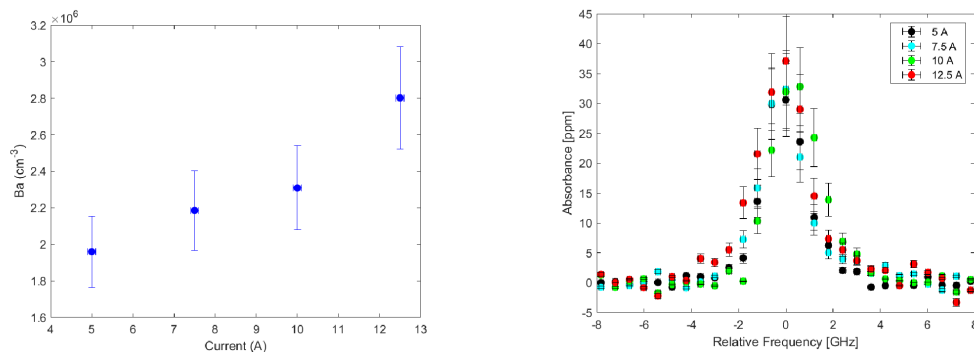
7

**Fig. 8** Left: Dependence of Ba density on cathode current at *r*=0, *z*= 5 mm, and flow rate=10 sccm. Right: Spectral scans corresponding to the current variation (after baseline subtraction).

In figure 9, the dependence of barium density on anode flow is shown. The flow rate is stepped in 10 sccm increments from 10 sccm to 40 sccm. Barium densities are again reported as ±20%, based on reproducibility. The uncertainty in flow rates is on the order of ±1% due to the rating of the mass flow controller. Measurements were performed at position of *r*=0 mm and *z*=5 mm at two current conditions of 5 and 12.5 A. The 5 A current shows overall gradually increasing barium densities with flow rate until the transition from 30 to 40 sccm occurs, which is a larger ~180% increase. For the 12.5 case, there is also initially an increase in Ba density with flow rate, but this is followed by a rapid drop as the flow rate increases from 20-30 sccm. We note that the visible appearance of the plume changes significantly in shape and appearance as this condition is varied with the most luminous region of plasma appearing to shift away from the CRDS probe beam location. Further experimental study, including imaging and spatial CRDS scans, will be needed to unravel these effects.
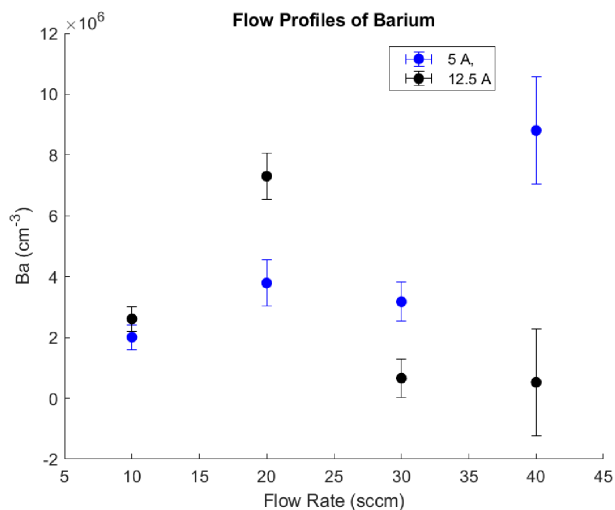


**Fig. 9** Dependence of Ba density on cathode flow rate at *r*=0 for currents of 5 and 12.5 A.

## V. Conclusions and Future Work

In this paper, we have shown the use of CRDS as a barium density measurement tool in a BaO HC plasma of varying conditions, including position in the plume over two dimensions, anode current, and flow rate of krypton. Overall, the closer in proximity to the HC orifice the probe beam is, the greater the barium levels are. This study allows the emission of barium to be understood for BaO HCs in support of numeric modeling and lifetimes studies. Taking radial scans allows the use of an Abel inversion to characterize the radially dependent density, and using this technique would allow further understanding of the plume under operating parameters of interest. Varying the height, current and flow parameters show the ability to understand the densest regions of barium, and the potential for high-density regions to shift under various operating conditions.

Future work will characterize the radial profiles at differing height, current, and flow parameters. We will also further examine the details of the CRDS spectra, in particular whether diagnostic information can be gleaned from the measured lineshape. Also of interest will be to attempt CRDS measurements along the axis of the cathode as well as to measure $Ba^+$ ions.

### References

[1] Goebel, D. M., and Katz, I., "Fundamentals of Electric Propulsion: Ion and Hall Thrusters," California Institute of Technology, 2008.

[2] Polk, J., Anderson, J., Brophy, J., Rawlin, V., Patterson, M., Sovey, J., and hamley, J., "An Overview of the Results from an 8200 Hour Wear Test of the NSTAR Ion Thruster," 1999. https://doi.org/10.2514/6.1999-2446

[3] Lee, B. C., Yalin, A. P., Gallimore, A., Huang, W., and Kamhawi, H., "Real-Time Boron Nitride Erosion Measurements of the HiVHAc Thruster via Cavity Ring-Down Spectroscopy," presented at the International Electric Propulsion Conference, IEPC-2013-119, 2013.

[4] Lee, B. C., Huang, W., Tao, L., Yamamoto, N., Gallimore, A. D., and Yalin, A. P., "A Cavity Ring-down Spectroscopy Sensor for Real-Time Hall Thruster Erosion Measurements," *Review of Scientific Instruments*, Vol. 85, No. 5, 2014, p. 053111. https://doi.org/10.1063/1.4879135

[5] Tao, L., Yamamoto, N., Gallimore, A. D., and Yalin, A. P., "Development of a Cavity Ring-down Spectroscopy Sensor for Boron Nitride Sputter Erosion in Hall Thrusters," 2010. https://doi.org/10.48550/ARXIV.1005.0592

[6] Yamamoto, N., Tao, L., Rubin, B., Williams, J. D., and Yalin, A. P., "Sputter Erosion Sensor for Anode Layer-Type Hall Thrusters Using Cavity Ring-Down Spectroscopy," *Journal of Propulsion and Power*, Vol. 26, No. 1, 2010, pp. 142–148. https://doi.org/10.2514/1.44784

[7] Huang, W., Gallimore, A. D., Smith, T. B., and Yalin, A. P., "The Technical Challenges of Using Cavity Ring-Down Spectroscopy to Study Hall Thruster Channel Erosion," 2011.

[8] Yalin, A. P., Surla, V., and Williams, J. D., "Erosion Measurements by Cavity Ring-Down Spectroscopy for the VHITAL Program," 2005.

[9] Yalin, A. P., Tao, L., Sullenberger, R. M., Oya, M., Yamamoto, N., Smith, T. B., and Gallimore, A. D., "High-Sensitivity Boron Nitride Sputter Erosion Measurements by Continuous-Wave Cavity Ring-Down Spectroscopy," 2008.

[10] Yalin, A. P., Surla, V., Butweiller, M., and Williams, J. D., "Detection of Sputtered Metals with Cavity Ring-down Spectroscopy," *Appl. Opt.*, Vol. 44, No. 30, 2005, pp. 6496–6505. https://doi.org/10.1364/AO.44.006496

[11] Dragnea, H. C., Boyd, I. D., Lee, B. C., and Yalin, A. P., "Characterization of Eroded Boron Atoms in the Plume of a Hall Thruster," *IEEE Transactions on Plasma Science*, Vol. 43, No. 1, 2015, pp. 35–44. https://doi.org/10.1109/TPS.2014.2320851

[12] Lee, D.-H., Yoon, Y., Kim, B., Lee, J. Y., Yoo, Y. S., and Hahn, J. W., "Optimization of the Mode Matching in Pulsed Cavity Ringdown Spectroscopy by Monitoring Non-Degenerate Transverse Mode Beating," *Applied Physics B: Lasers and Optics*, Vol. 74, Nos. 4–5, 2002, pp. 435–440. https://doi.org/10.1007/s003400200802

[13] Maity, A., Maithani, S., and Pradhan, M., "Cavity Ring-Down Spectroscopy: Recent Technological Advancements, Techniques, and Applications," *Analytical Chemistry*, Vol. 93, No. 1, 2021, pp. 388–416. https://doi.org/10.1021/acs.analchem.0c04329

[14] Kramida, A., and Ralchenko, Y., "NIST Atomic Spectra Database, NIST Standard Reference Database 78," National Institute of Standards and Technology, 1999. https://doi.org/10.18434/T4W30F

[15] Killer, C., "Abel Inversion Algorithm," MATLAB Central File Exchange, 2023. Retrieved 10 December 2023. (https://www.mathworks.com/matlabcentral/fileexchange/43639-abel-inversion-algorithm